A Method of Orbit Determination Using Overlapping Television Pictures

J. K. CAMPBELL*
Jet Propulsion Laboratory, California Institute of Technology, Pasadena, Calif.

A method that utilizes the Mariner Mars 1969 television pictures has been developed to aid in the post-encounter determination of the TV viewing directions. A weighted least-squares estimation scheme is used, based on observation of common Mars surface features in overlapping TV pictures. Estimates were also obtained for the encounter orbits of Mariners VI and VII, and also for the orientation of the Mars spin axis; however, the estimated solutions for the spacecraft orbits and for the spin axis did not result in a reduction of the a priori uncertainties in these parameters. Good results were obtained for the estimated corrections and the a posteriori uncertainties of the nominal TV viewing directions.

Introduction

TO determine the locations on Mars of the Mariner near-encounter TV pictures, accurate determinations of the camera viewing directions are required. Also required are accurate determinations of the encounter orbits and the orientation of the Mars spin axis. Highly accurate estimates of the camera pointing angles can be obtained from telemetered readouts of the commanded angle settings and spacecraft attitude. However, the Mariner VII spacecraft experienced an anomaly shortly before arriving at Mars. The anomaly corrupted the radio tracking data for a short time and damaged the telemetry channel which described one of the camera pointing angles. Thus, a need arose to refine the nominal encounter estimates of the Mariner VII camera pointing angles.

A method was developed for estimating corrections to the nominal camera pointing angles, and also the spacecraft encounter orbits and the Mars spin axis. The method utilizes the overlapping television pictures which were obtained during each Mariner '69 flyby, and the weighted-least-squares estimation technique. Solutions were obtained for both Mariner VI and VII parameters.

The method can be summarized as follows. In two or more overlapping TV pictures, one identifies a number of surface features which lie in the overlap region. The picture coordinates of each feature in each picture are then measured. The aerocentric latitude and longitude of each feature in each overlapping picture are computed from the measured coordinates and a set of nominal parameters which describe the camera orientation, the times of the picture shutterings, the spacecraft orbit, and the Mars spin axis and planet radius. The same feature in two or more pictures should have the same computed values of latitude and longitude. However, differences in the computed values will result because of the presence of errors in the nominal parameter values, and the picture measurement errors.

The presence of these a priori errors and feature measurement noise are accounted for in a weighted-least-squares estimate of corrections to the nominal camera pointing angles, the spacecraft encounter orbits, and the Mars spin axis.

A total of seven parameters are considered in the model: three camera orientation angles, two components of the spacecraft orbit, and two angles that describe the orientation of the spin axis. The planet radius and the times of the picture shutterings have been well established, and are assumed to be known.

The next sections will define further the parameters of the solution model, review the least-squares equations, characterize the equations in terms of the parameters, and summarize the results obtained.

TV Camera Orientation Parameters

The TV camera is mounted on an instrument platform. The orientation of the instrument platform is defined in a spacecraft-fixed reference frame. The spacecraft fixed frame is, in turn, optically referenced to the sun and the star Canopus through error signals from the sun sensors and the Canopus tracker. The reference angles for the platform orientation are referred to as clock, cone, and twist angles (KA, CA, TA). An ordered rotation of the spacecraft axes

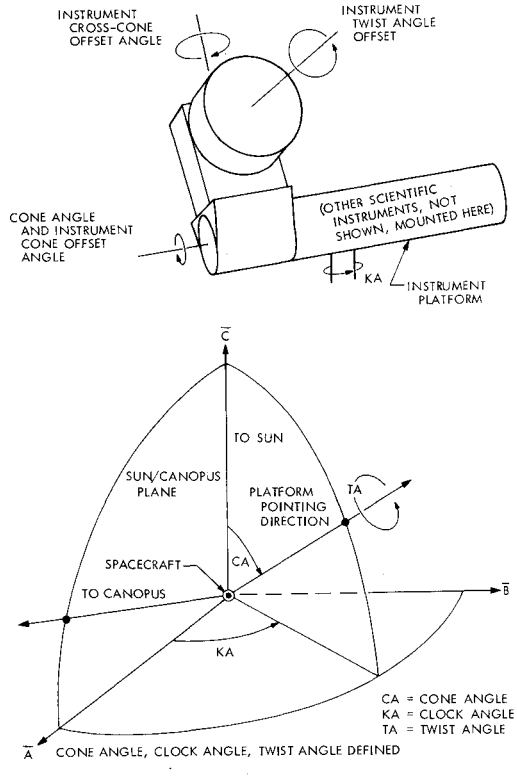

Fig. 1 Definition of camera orientation parameters.

Presented as Paper 70-1066 at the AAS/AIAA Astrodynamics Conference, Santa Barbara, Calif., August 19-21, 1970; submitted September 11, 1970; revision received March 31, 1971. This paper presents the results of one phase of research carried out at the Jet Propulsion Laboratory, California Institute of Technology, under Contract NAS 7-100, sponsored by NASA.

* Cognizant Trajectory Engineer for Mariner Mars 1969, and Member of Navigation and Mission Design Section.

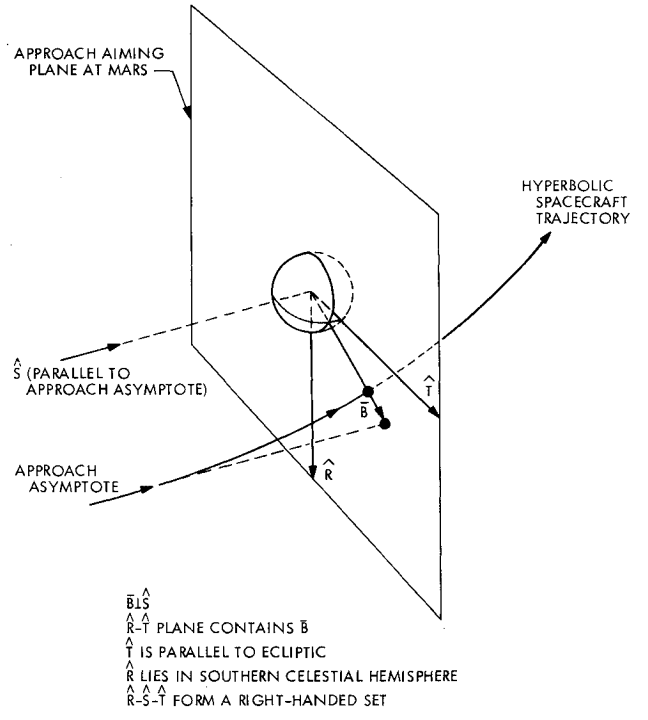

Fig. 2 Definition of encounter trajectory parameters.

through the angles (clock, cone, twist) produces the platform-fixed reference frame in which the TV optic axis is defined. In the platform-fixed reference frame, the TV camera coordinate frame is referenced by the cone offset, cross-cone offset, and twist offset angles. An ordered rotation of the platform reference frame through the angles (cone offset, cross-cone offset, twist offset) produces the inertial definition of the TV camera coordinate frame. Figure 1 illustrates the reference frames.

The instrument platform had only two *commanded* degrees of freedom relative to the spacecraft fixed axes. These were the clock and cone angle settings sent to the spacecraft. The platform twist angle resulted from spacecraft-platform mounting misalignments and from the component of spacecraft attitude motion which resolves along the twist axis.

The offsets of the optic axis in the platform reference frame were calibrated and are assumed to be known. The cone, clock, and twist angles of the platform relative to the spacecraft inertial axes are solved for in the model.

Spacecraft Encounter Orbit Parameters

The encounter orbit (well approximated by an aerocentric hyperbola) can be defined by six orbital elements, as well as several physical constants which enter into the description of the motion. A particular set of parameters commonly used at the Jet Propulsion Laboratory is the following (see Fig. 2): 1) the (inertial) direction of the parallel $\hat{\mathbf{S}}$ to the approach asymptote, 2) the speed along the asymptote V_∞ and time of closest approach, and 3) the "miss vector" $\bar{\mathbf{B}}$ defining the inertial position of the approach asymptote.

The vector $\hat{\mathbf{S}}$, the speed along the asymptote V_∞, and the time of closest approach are assumed known. These parameters have been well determined for both Mariner VI and VII encounter orbits from cruise phase radio-tracking solutions.[1] The various physical constants are also assumed to be known.[2] The remaining parameter is the vector $\bar{\mathbf{B}}$. The components of $\bar{\mathbf{B}}$, $\bar{\mathbf{B}}\cdot\hat{\mathbf{T}}$ and $\bar{\mathbf{B}}\cdot\hat{\mathbf{R}}$, are solved for in the model.

Model Parameters and Dependent Variables

The model used to represent the picture locations on the Mars surface is characterized by the following parameters (independent variables): α = right ascension of Mars spin axis, δ = declination of Mars spin axis, $\bar{\mathbf{B}}\cdot\hat{\mathbf{T}}$,$\bar{\mathbf{B}}\cdot\hat{\mathbf{R}}$ = components of $\mathbf{B}$ vector, CA,KA,TA = cone, clock, twist angle, respectively, defining instrument platform pointing direction.

The dependent variables (observables) that were chosen are the latitude differences and longitude differences between the assumed common surface features. Thus, a single common point which is located in two pictures will produce two observables, a latitude difference and a longitude difference. A point located in three pictures produces six observables. In general, the number of observables for a given set of overlapping pictures is

$$N = 2\sum_{q=1}^{Q} F_q P_q$$

where F_q is the number of features chosen which appear in P pictures, within overlap q, and Q is the total number of overlap regions considered.

One result of using longitude differences is the uncoupling of the right ascension and declination of the Mars pole from longitude coordinates of the features, which are dependent on the hour angle of the Mars equinox. Longitude differences, however, are independent of the hour angle, which is changed by a correction to the spin axis declination or right ascension.

The (spherical) radius of the planet was fixed, hence only two degrees of freedom have been allowed for the surface points. The estimation of local surface elevations requires the use of stereoscopic feature measuring equipment, which was not available for this preliminary effort. The neglect of these elevation variations is estimated to have only small effects on feature location measurements.

Estimation Equations

A standard nonrecursive weighted-least-squares estimation scheme is used to estimate the parameters. The equations defining the weighted-least-squares estimation technique can be summarized as follows:

Given the linear matrix equation

$$\bar{\mathbf{y}} = A\bar{\mathbf{x}} + \bar{\boldsymbol{\epsilon}}$$

the best estimate, in the weighted-least-squares sense, for the corrections to the nominal parameter set is[3]

$$\bar{\mathbf{q}} = (A^T W A + \Gamma_x)^{-1} A^T W \bar{\mathbf{r}}$$

where $\bar{\mathbf{y}}$ = the $n \times 1$ known data vector, $\bar{\mathbf{x}}$ = the $m \times 1$ vector of solve-for parameters, $\bar{\boldsymbol{\epsilon}}$ = the $n \times 1$ unknown observation error vector, A = the $n \times m$ known matrix of coefficients with $n \geq m$, $\bar{\mathbf{q}}$ = the $m \times 1$ estimated correction vector, $\bar{\mathbf{r}}$ = the $n \times 1$ residual vector, W = the $n \times n$ diagonal matrix of data weighting coefficients, and Γ_x = the $m \times m$ diagonal matrix of parameter weighting coefficients.

The columns of A represent the partial derivatives of the observables with respect to each independent variable. These partials were computed by numerical differencing.

Characterization of Equations

The Residual Vector

The residual vector $\bar{\mathbf{r}}$ is defined to be the $n \times 1$ vector of observed-minus-computed values of the dependent variables. This vector is non-zero because of the presence of errors in estimating the nominal parameter set, and measurement errors in the picture coordinates. However, because of the definition of the observables as the latitude and longitude differences between assumed common features, the "observed"

component of $\bar{\mathbf{r}}$ is identically zero. (Since one is observing assumed common surface features in several pictures, by definition one observes the surface coordinates of the common features to be identical.) Thus, the $\bar{\mathbf{r}}$ vector is the negative of the computed latitude and longitude differences between the common features.

Computation of Weighting Matrix W

The diagonal elements of W are taken to be the inverse of the squared error or standard deviation on each observable. The off-diagonal terms are dropped because of the small correlation coefficients; hence the W matrix is diagonal.

The elements of W are computed by mapping the uncorrelated feature measurement errors into errors in the latitude and longitude differences for each overlapping picture. For a feature in a single picture, the covariance matrix of 1-σ latitude and longitude errors is

$$\Lambda = M\Lambda_m M^T$$

where Λ_M is the diagonal matrix of 1-σ measurement errors and M is the mapping matrix. The errors in the overlapping picture are independent, so that the error in the latitude and longitude differences is obtained by combining the latitude and longitude errors from each picture. Thus, the 1-σ error made in estimating the latitude difference between overlapping pictures A and B is

$$\sigma_{\text{lat}} = \sigma_m[(\sigma_{\text{lat}_A})^2 + (\sigma_{\text{lat}_B})^2]^{1/2}$$

and the longitude difference error is

$$\sigma_{\text{long}} = \sigma_m[(\sigma_{\text{long}_A})^2 + (\sigma_{\text{long}_B})^2]^{1/2}$$

where σ_m is the standard deviation of the feature measurement error.

The mapping matrix M is defined by

$$M = \begin{bmatrix} M_x(\hat{\mathbf{E}}\cdot\hat{\mathbf{x}}) & M_y[(\hat{\mathbf{E}}\cdot\hat{\mathbf{y}}) \\ M_x(\hat{\mathbf{N}}\cdot\hat{\mathbf{y}}) & M_y[(\hat{\mathbf{N}}\cdot\hat{\mathbf{y}}) \end{bmatrix}$$

where $\hat{\mathbf{E}},\hat{\mathbf{N}}$ = unit vectors to local east, north directions, projected onto the image plane, $\hat{\mathbf{x}},\hat{\mathbf{y}}$ = unit vectors defining the feature measurement reference directions, and M_x,M_y = coefficients relating unit distances in x,y directions to the corresponding angle at the planet surface.

The vectors $\hat{\mathbf{E}},\hat{\mathbf{N}}$ are computed by

$$\hat{\mathbf{E}} = \hat{\mathbf{C}} \times \left[\frac{\hat{\mathbf{P}} \times \hat{\mathbf{R}}}{|\hat{\mathbf{P}} \times \hat{\mathbf{R}}|} \times \hat{\mathbf{P}}\right], \text{ unitized}$$

$$\hat{\mathbf{N}} = \hat{\mathbf{C}} \times \left[\left(\hat{\mathbf{R}} \times \frac{\hat{\mathbf{P}} \times \hat{\mathbf{R}}}{|\hat{\mathbf{P}} \times \hat{\mathbf{R}}|}\right) \times \hat{\mathbf{P}}\right], \text{ unitized}$$

where $\hat{\mathbf{C}}$ = unit vector along the optic axis, $\hat{\mathbf{P}}$ = unit vector along the optic path which intercepts the measured feature at the planet surface, $\hat{\mathbf{R}}$ = unit vector along the planet-centered direction to the measured feature, and $\hat{\mathbf{P}}$ = unit vector in the direction of the Mars north pole.

The coefficients M_x,M_y are computed by

$$M_x = [R_S(\hat{\mathbf{p}}\cdot\hat{\mathbf{C}})/F(\hat{\mathbf{p}}\cdot\hat{\mathbf{R}})]|(\hat{\mathbf{p}} \times \hat{\mathbf{x}}) \times \hat{\mathbf{R}}|(k/R_p)$$

$$M_y = [R_S(\hat{\mathbf{p}}\cdot\hat{\mathbf{C}})/F(\hat{\mathbf{p}}\cdot\hat{\mathbf{R}})]|(\hat{\mathbf{p}} \times \hat{\mathbf{y}}) \times \hat{\mathbf{R}}|(k/R_p)$$

where R_S = range to the surface along the optic path to the measured feature, R_p = (spherical) radius of planet, F = camera focal length and k = radians-to-degrees factor.

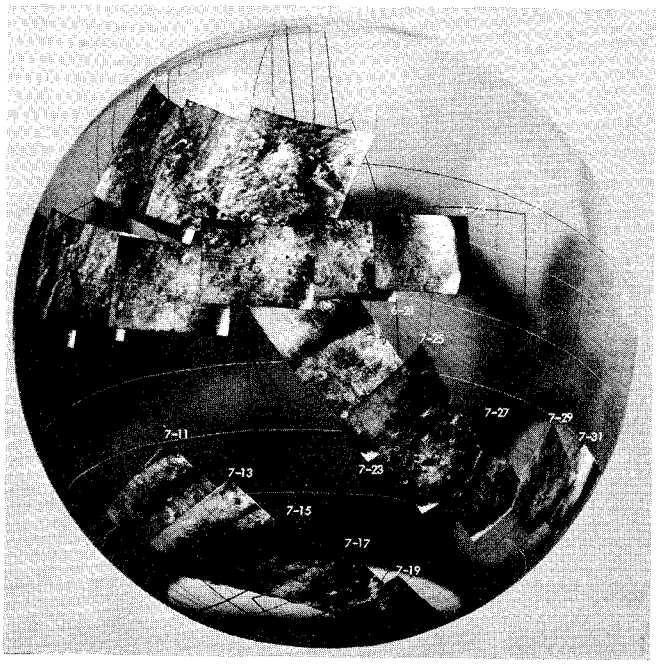

Fig. 3 Globe with mosaics of Mariner VI and Mariner VII wide-angle TV pictures.

The Parameter Weighting Matrix Γ_x

The diagonal elements of Γ_x are the inverse of the 1-σ uncertainties in each independent variable. The parameters are assumed to be uncorrelated; hence Γ_x is diagonal. The uncertainties are estimated from the consideration of radio-tracking orbit estimates in the case of $\bar{\mathbf{B}}\cdot\hat{\mathbf{T}}$ and $\bar{\mathbf{B}}\cdot\hat{\mathbf{R}}$; from consideration of telemetry measurement and resolution errors in the platform angles CA, KA, TA; and from consideration of various previous estimates for the spin axis coordinates α,δ.

Description of Pictures and Measurements

The nominal TV picture map[4] for each encounter is shown in Fig. 3. The Mariner VI pictures are in the upper two rows of the figure. (Initial portions of the mosaic are shown lined in to avoid confusion.) Mariner VI took 24 close-range photos of the surface, 12 narrow-angle (nested within overlap regions, and not shown) and 12 wide-angle pictures. The 25th picture was taken on the night side of the day/night terminator. Photo 21 was taken at nearly the closest range, 3428 km. Mariner VII took 17 wide-angle and 16 narrow-angle pictures during its close passage of Mars. Picture 30 was taken at nearly the closest range, 3440 km. The pictures were shuttered with the instrument platform in several different orientations during the flybys, with cone angle settings ranging from 100°–145° and clock angles settings from about 215°–270° for both platforms. The pictures were shuttered on 42.2-s centers, with the wide-angle picture, shuttered every 84.4 s.

The Mariner VI TV pictures which were used (Fig. 4) generally are photographs of desert areas. Craters are clearly visible in the areas of Margaritifer Sinus (top left), Meridiani Sinus (top center), and Deucalionis Regio (lower strip). Locations of three narrow-angle pictures are marked by rectangles. North is approximately toward the top, and the sunset terminator lies near the right edge of frame 6N23. Common feature identification in the Mariner VI pictures was more difficult than in the Mariner VII pictures used (Fig. 5), which contain many features at the boundary of the south polar cap.[5] The south pole lies near the parallel streaks in the lower right corner of frame 7N17.

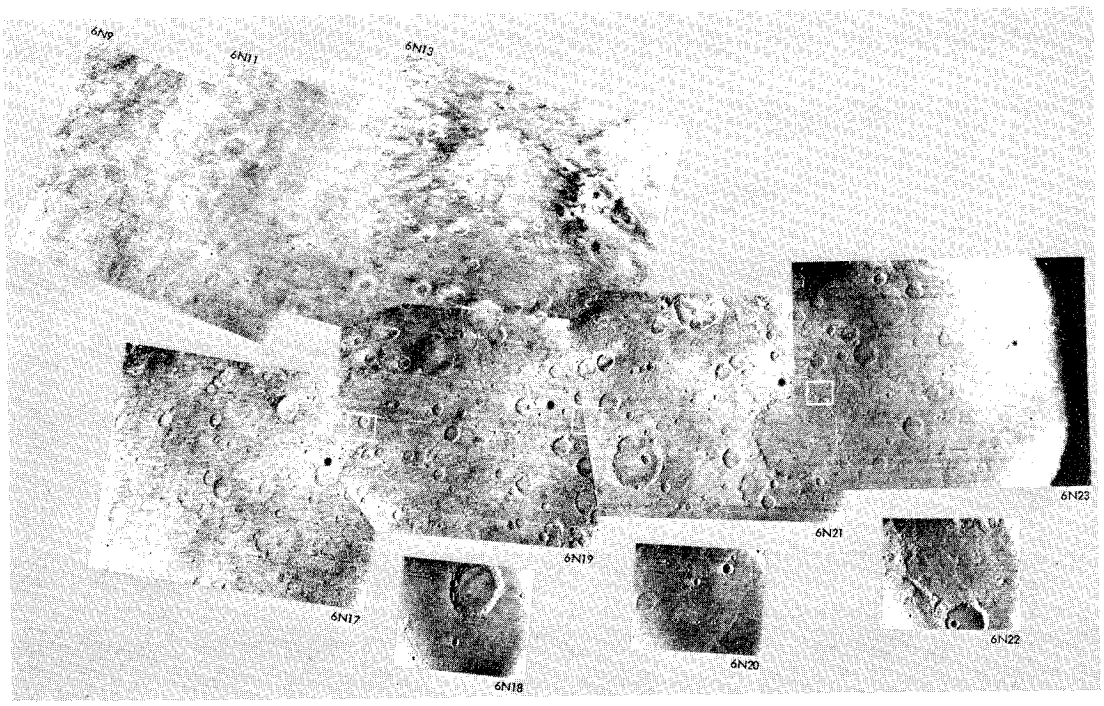

Fig. 4 Mosaic of ten Mariner VI pictures.

The wide-angle TV pictures were used to obtain common surface features. The nature of the selected features is of no consequence, so long as they remain planet-fixed during the picture-taking sequence and can be accurately identified in each overlapping picture. In general, the common features were chosen to be small portions of crater ridges and other easily recognizable areas. One must be careful not to choose features which may actually be, for example, atmospheric clouds, surface shadows, or electronic distortions. Twenty surface features were identified and measured in the Mariner VI pictures and fifteen in the Mariner VII pictures.

The locations of the common features were then measured in each TV picture. The measurements are made in picture coordinates, which may generally be defined by any convenient unit that relates the picture coordinates with the camera focal length, in order to calculate the optic ray which inter-

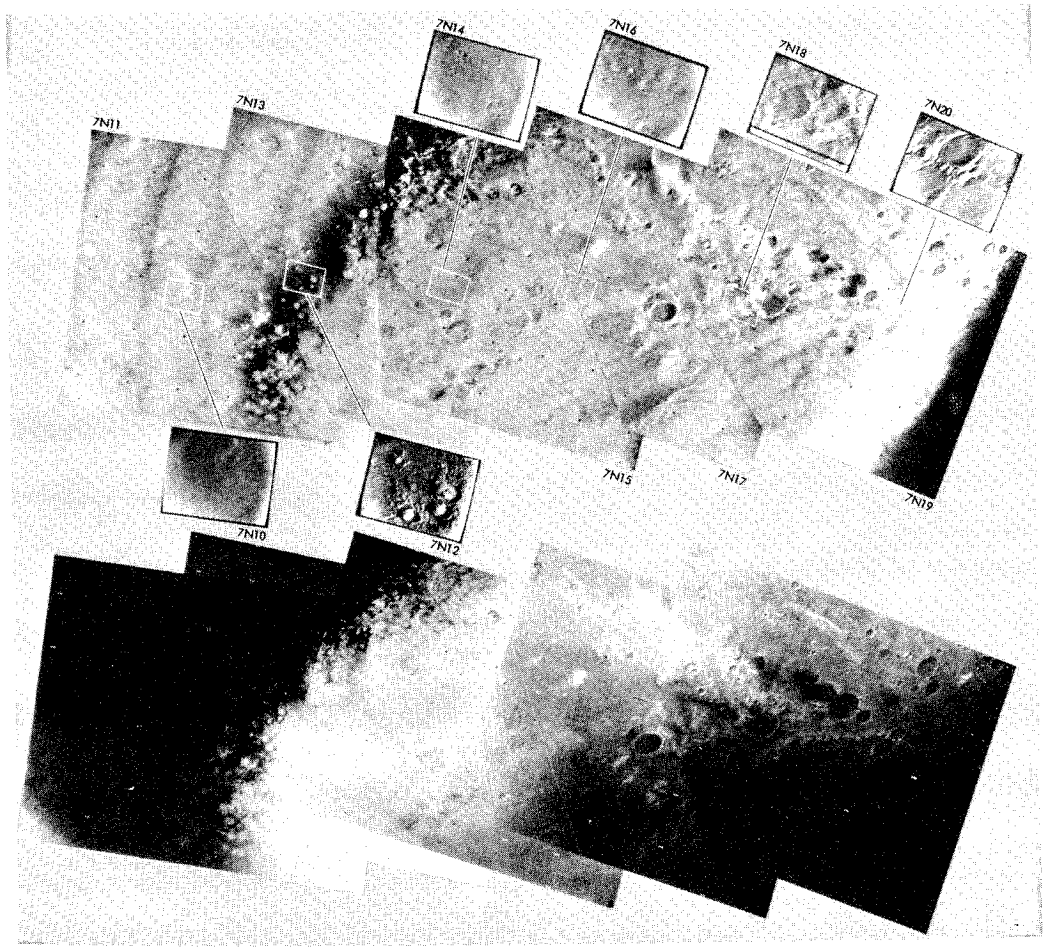

Fig. 5 Mosaic of eleven Mariner VII polar cap pictures.

Table 1 Average residuals for Mariner VI and VII overlap regions

Overlap region	Pictures	Latitude residual, deg		Longitude residual, deg	
		A priori	Corrected	A priori	Corrected
6A	9,11	+0.19	+0.25	−0.24	+0.20
6B	11,13	−0.53	−0.47	−0.07	−0.06
6C	19,21	−0.16	−0.01	−0.002	−0.01
6D	21,23	−0.16	−0.01	+0.01	−0.01
7A	11,13	+0.13	−0.02	+0.29	+0.29
7A	11,15	+0.36	+0.06	+0.21	+0.29
7A	13,15	+0.23	−0.09	−0.08	−0.19
7B	13,15	+0.25	−0.02	−0.06	−0.04
7B	13,17	+0.09	−0.04	−0.01	−0.002
7B	15,17	−0.16	−0.19	+0.03	+0.04
7C	15,17	−0.14	−0.20	+0.49	+0.38
7C	15,19	−0.22	−0.35	+0.25	+0.13
7C	17,19	−0.08	−0.15	−0.24	−0.25

cepts the feature. The pictures have a grid superimposed during processing, with the grid unit of 5 pixels, where a pixel is a picture element.[4] The grid size for each wide-angle frame is approximately 1000 × 775 pixels, and the field of view is about 14° × 11°. The focal length of each wide-angle camera was approximately 52 mm. Calibration and reduction of appropriate TV test data[6] produced the pixel/millimeter factor necessary to express the camera focal length in picture coordinate units. The coordinates are referenced to the nominal optic axis intercept on the focal plane, that is, the optical center of the picture frame.

Results

The essential results of the estimation scheme are shown in Tables 1 and 2. The results have been summarized from analysis and interpretation of the a posteriori residuals listed in Table 1, and the stability and sensitivity of the solutions when the data and data weights are varied. The absence of an entry in Table 2 indicates that a poor solution was obtained for that overlap region. Note that in all solutions for the Mars spin axis coordinates (α,δ), the a prioriuncertainty was not improved. Also note that the corrections to the orbit parameters ($\bar{\mathbf{B}}\cdot\hat{\mathbf{T}}$, $\bar{\mathbf{B}}\cdot\hat{\mathbf{R}}$) are of the same order of magnitude as their estimated uncertainties.

A strong positive twist angle bias appears to exist in the nominal Mariner VI platform angles. Davies and Berg[7] have confirmed this finding, using both full-disk and closeup pictures. Their analysis was cartography-oriented and was based on the use of many more surface features and a refined measuring technique. They explain this bias as being due to a small angle between the TV scan lines and the reference grid on the face of the vidicon. The scan lines were used to align the picture coordinate grid and thus implicitly define the camera twist angle, whereas the reference grid was used to calibrate the camera twist angle.

An independent technique used by the author infers the same platform angle corrections as those reported in Table 2. In a nominal set of computer-drawn encounter pictures,[8] platform angle corrections were calculated to match the planet limbs with the limbs in the actual pictures.[9] The calculated corrections verified the platform angle corrections listed in Table 2.

Summary

The results for the platform angle corrections were encouraging for both spacecraft. Note that the corrections that were solved for are for bias corrections which essentially shift the pictures in a given overlap region in a uniform manner. A much larger number of measured surface features would allow a solution for the viewing direction of each picture relative to the pictures with which it overlaps. An inertial viewing direction for each picture could then be estimated using the present scheme. The viewing directions would be independent of the actual Mars-fixed coordinates of any surface feature.

The spin axis solutions were weak because of the small planet and spacecraft angular motion during each of the picture sequences. Estimates for the spin axis are most accurate when the planet rotates 90° between overlapping picture shutterings. The periodic motion of the spacecraft due to attitude control requires a relatively long areocentric trajectory arc to effectively solve for the orbit parameters $\bar{\mathbf{B}}\cdot\hat{\mathbf{T}}$ and $\bar{\mathbf{B}}\cdot\hat{\mathbf{R}}$. Generally speaking, an optimal set of solutions for the camera angles is obtained when the viewing angle between pictures is approximately 90°.

The results of the preliminary effort discussed in this paper indicate that the development of a general capability for geometrically processing TV and other instrument data will significantly enhance the scientific return from future interplanetary missions. Improved knowledge of the elements of the Mars satellite orbits results from the use of photos which contain the satellites.[10]

References

[1] Gordon, H. J. et al., "The Mariner VI and VII Flight Paths and Their Determination From Tracking Data," TM 33-469, Dec. 1970, Jet Propulsion Lab., Pasadena, Calif.

[2] Melbourne, W. G. et al., "Constants and Related Information for Astrodynamic Calculations," TR 32-1306, July 1968, Jet Propulsion Lab., Pasadena, Calif.

Table 2 Estimated corrections and 1-σ correction uncertainty[a]

Overlap regions	Parameters estimated						
	α, 1.0[b]	δ, 1.0[b]	$\bar{\mathbf{B}}\cdot\hat{\mathbf{T}}$, 10 km[b]	$\bar{\mathbf{B}}\cdot\hat{\mathbf{R}}$, 10 km[b]	CA, 0.3[b]	KA, 0.3[b]	TA, 0.3[b]
6A,B	0.15	0.45			0.40	−0.20	−1.30
	(1.0)	(1.0)			(0.25)	(0.15)	(0.10)
6C,D	0.10	0.20	3.0 (6.0)	−2.0 (6.0)	−0.10	−0.10	−0.75
	(1.0)	(1.0)			(0.25)	(0.15)	(0.10)
6A,B,C,D	0.10	0.15			0.05	−0.30	−1.0
	(1.0)	(1.0)			(0.15)	(0.15)	(0.10)
7A					0.60	0.30	0.85
					(0.08)	(0.20)	(0.08)
7B	0.60	0.40	−5.0 (9.0)	3.0 (9.0)	0.10	0.10	0.20
	(1.0)	(1.0)			(0.10)	(0.10)	(0.20)
7C					−0.40		−0.80
					(0.05)		(0.10)
7A,B,C					−0.20	0.60	1.20
					(0.05)	(0.20)	(0.15)

[a] 1-σ correction uncertainty in parentheses.
[b] A priori uncertainty in deg., except as shown.

[3] Anderson, J. D., "Theory of Orbit Determination—Part II, Estimation Formulas," TR 32-498, Oct. 1963, Jet Propulsion Lab., Pasadena, Calif.
[4] Leighton, R. B., "The Surface of Mars," *Scientific American*, May 1970, Vol. 222 No. 5 pp. 26-41.
[5] Sharp, R. P. et al., "The Surface of Mars 4. South Polar Cap," *Journal of Geophysical Research*, Vol. 76, Jan. 1971, pp. 357-368.
[6] Danielson, G. E. and Montgomery, D. R., "Calibration of the Mariner Mars 1969 Television Cameras," *Journal of Geophysical Research*, Vol. 76, Jan. 1971, pp. 418-431.
[7] Davies, M. E. and Berg, R. A., "A Preliminary Control Net of Mars," *Journal of Geophysical Research*, Vol. 76, Jan. 1971, pp. 373-393.
[8] Campbell, J. K., "Mariner Mars 1969 Simulated Television Pictures—Final," Internal Document 605-237, June 1970, Jet Propulsion Lab., Pasadena, Calif.
[9] Dunne, J. A. et al., "Maximum Discriminability Versions of the Near-Encounter Mariner Pictures," *Journal of Geophysical Research*, Vol. 76, Jan. 1971, pp. 438-472.
[10] Duxbury, T. C., "A Spacecraft-Based Instrument for Outer-Planet Missions," AIAA Paper 69-902, Princeton, N.J., 1969.

AUGUST 1971 J. SPACECRAFT VOL. 8, NO. 8

Analytic Difficulties in Predicting Dynamic Effects of Separated Flow

LARS E. ERICSSON,* J. PETER READING,† AND ROLF A. GUENTHER‡
Lockheed Missiles & Space Company, Sunnyvale, Calif.

The purpose of the paper is to demonstrate how a simple analytic theory that uses static experimental data as an input, can predict the observed large adverse effects of separated flow on the vehicle dynamics of heat-sink type re-entry bodies and elastic launch vehicles. The theory is based on quasi-steady-flow concepts in which the time history effects are lumped to one discrete past time event. The analytic difficulties consist largely of insufficient capability in predicting the composition of static loads in regions of separated flow, even when static experimental data are available. If more basic knowledge were available about nonsymmetric stationary separated flow, very substantial improvement in existing capability to predict dynamic effects of separated flow would result.

Nomenclature

A = axial force, kg, coefficient $C_A = A/(\rho U^2/2)S$
c = reference length, m (usually $c = d$)
d = body caliber, m
N = normal force, kg, coefficient $C_N = N/(\rho U^2/2)S$
L = longitudinal wake source distance, m
M = Mach number
M_P = pitching moment, kg-m, coefficient $C_m = M_P/(\rho U^2/2)Sc$
p = static pressure, kg/m^2
C_p = pressure coefficient $C_p = (p - p_\infty)/(\rho U^2/2)$
S = reference area, m^2, $S = \pi c^2/4$
t, Δt = time, and time lag, respectively, sec
U = freestream velocity, m/sec
$\bar{U}$ = mean convection velocity, m/sec
x,z = horizontal and vertical coordinates, respectively, m
ξ = dimensionless x coordinate, $\xi = x/c$
α = angle of attack, rad or deg
α_0 = trim angle of attack, rad or deg
β = equivalent spike deflection angle, rad or deg
Δ = difference
δ_F = flare rotation angle, rad or deg
ρ = air density, kg-sec^2/m^4
ω = pitching or bending frequency, rad/sec
$\bar{\omega}$ = reduced frequency, $\bar{\omega} = \omega c/U$
θ = body attitude, rad or deg

Subscripts

a = attached flow
C = cylinder
N = nose
QS = quasi-steady
s = separated flow
∞ = undisturbed flow

Superscripts

i = induced, e.g., $\Delta^i C_N$ = separation induced normal force
$'$ = induced by upstream communication, e.g., $C_{N_{\alpha'_s}}$
$\sim$ = generalized or effective value, e.g., $\tilde{\alpha}$

Differential symbols

$\dot{\theta}(t) = \partial\theta/\partial t$
$C_{N_\alpha} = \partial C_N/\partial\alpha$; $C_{m_\beta} = \partial C_m/\partial\beta$; $C_{N_\theta} = \partial C_N/\partial\theta$

Presented as Paper 70-762 at the AIAA 3rd Fluid and Plasma Dynamics Conference, Los Angeles, Calif., June 29–July 1, 1970; submitted August 6, 1970; revision received February 24, 1971.

* Senior Staff Engineer. Associate Fellow AIAA.
† Research Specialist. Member AIAA.
‡ Senior Aerodynamics Engineer.

Introduction

BOTH ascent and re-entry vehicles exhibit large regions of separated flow, especially in the transonic Mach number range. Heat-sink type re-entry bodies and the Saturn-Apollo launch vehicles exemplify cases where the aerodynamic loading is generated by "separated flow with embedded regions of attached flow." It is a well-known fact that simulation of boundary-layer separation and wake formation in a wind tunnel is very difficult for stationary flow, and is practically impossible in many cases for unsteady separated flow. As neither theory nor experiments alone can provide a solution, using both in combination is the only realistic approach.

Analysis

Quasi-steady forces are essentially static forces modified to account for slow perturbations from the static condition. The required slowness, $\bar{\omega}^2 \ll 1$, to make quasi-steady treatment applicable is fulfilled for rigid body oscillations of ascent and re-entry vehicles, and for elastic vehicle oscilla-